Computers and Structures 157 (2015) 218–231

Contents lists available at ScienceDirect

Computers and Structures

journal homepage: www.elsevier.com/locate/compstruc

Modeling steel structures in OpenSees: Enhancements for fire and multi-hazard probabilistic analyses

Negar Elhami Khorasani *[a], Maria E.M. Garlock [a], Spencer E. Quiel [b]

[a] Dept. of Civil and Environmental Engineering, Princeton University, Princeton, NJ, United States
[b] Dept. of Civil and Environmental Engineering, Lehigh University, Bethlehem, PA, United States

ARTICLE INFO

Article history:
Received 17 July 2014
Accepted 19 May 2015

Keywords:
OpenSees
Thermal analysis
Constitutive material model
Strain reversal
Fire-following-earthquake
Reliability

ABSTRACT

Fire and post-earthquake fires pose a major hazard to our built environment with possible catastrophic consequences. Any framework developed for evaluating the resilience of steel structures in a multi-hazard context should incorporate tools that are capable of probabilistic structural analyses under fire and seismic loads. With a newly added thermal module, the OpenSees software has the capacity to perform structural analysis for the effects of cascading seismic and fire events. This paper presents modifications to the current source code that enable post-earthquake fire analysis for steel structures, and the enhancement to adapt reliability analysis in the thermal module.

1. Introduction

Fire following an earthquake (FFE) is a major hazard in densely populated urban areas in seismic regions. Documented historical examples of fires after an earthquake that have caused considerable structural damage include those associated with the San Francisco 1906 and 1989, Tokyo 1923, and Kobe 1995 seismic events [34]. While the occurrence of an earthquake and its consequences cannot be prevented, proper design of structures can certainly minimize the potential for damage. In a strong earthquake, buildings designed for seismic regions may experience plastic deformations but do not collapse. Fires following the earthquake, however, will further weaken the structure and can provide the catalyst for a more severe structural response. The likelihood of fire is typically amplified following seismic events due to an increase and/or introduction of available fuel and ignitions sources, such as ruptured utility lines or toppled appliances. Structural resistance to fire may be diminished as well. Active fire protection systems, such as sprinklers, may be ineffective due to ruptured water lines, loss of water pressure, or inadequate water supply due to widespread firefighting efforts for multiple neighboring fires. Passive fire protection systems, such as spray-applied materials or compartmentation partitions, can also be damaged and/or compromised by seismic vibration. When fire follows an earthquake, buildings with reduced strength or diminished fire resistance may not have the ability to resist the subsequent extreme event.

Previous research of structural performance for post-earthquake fires has typically studied the problem in separate programming environments for seismic and thermal analyses [8,39,30]. The shortcoming in such an approach is that switching between programs to complete seismic and thermal analyses requires certain idealizations, such as disregarding material and structural degradation after the earthquake, which would reduce the effectiveness of the modeling results. ABAQUS and DIANA are commercially available finite element programs which can be used to perform both seismic and thermal analyses; however, the structure of both programs requires extensive computational resources to perform one set of back-to-back seismic and fire analyses.

Another point to consider is that, although performance-based guidelines for seismic design of structures have been well established, the available design procedures for fire are fairly new and largely based on prescriptive codes [5,3] or performance-based guidelines with deterministic input variables [6,7,21]. Additionally, the available data shows that considerable uncertainty exists in defining fire load density and properties of material at elevated temperatures [9]. Therefore, a reliability approach to evaluating structures in fire is necessary, and consequently a finite element program that can effectively model fire and FFE while also incorporating uncertainties in the thermal analysis is needed. The

* Corresponding author.
E-mail addresses: nelhami@princeton.edu (N. Elhami Khorasani), mgarlock@princeton.edu (M.E.M. Garlock), squiel@lehigh.edu (S.E. Quiel).

http://dx.doi.org/10.1016/j.compstruc.2015.05.025
0045-7949/

computational resources and effort required to perform reliability analysis with a fire scenario in ABAQUS or DIANA are significant and diminish the feasibility of using either software package in this application.

OpenSees is a finite element program and object-oriented software that was developed at the University of California, Berkeley, mainly for nonlinear analysis of structures under seismic loadings [25]. In recent years, Professor Asif Usmani and his research team at the University of Edinburgh have been working on adding *structures in fire* modeling capacity to OpenSees [22,23]. The recently introduced thermal module is consistent with the object-oriented programming structure of the overall OpenSees software package. New classes for defining time–temperature relations were added to the code, and existing classes were modified to account for the effect of thermal load. OpenSees has the potential to run FFE analysis efficiently because it can perform both the seismic and structural-fire analyses. These analyses can be easily set up on high-performance computing hardware and can be modified by the user to include uncertainties in both the seismic and thermal parameters because it is an open-source code. At its current stage of development, however, the new module is not capable of performing back-to-back seismic and thermal analysis because the current constitutive material models cannot accommodate both hazards.

This paper proposes modifications to the thermal module of OpenSees with the objectives of (1) enhancing the code performance for fire analysis, (2) enhancing the constitutive material model to allow a seamless transfer from seismic to thermal analysis during FFE scenarios, and (3) enable reliability analysis within the thermal module analysis. The paper has two primary contributions:

- Modifications to the current steel material class in the thermal module of OpenSees are proposed in order to achieve the first two objectives. The implemented changes include an alteration of the constitutive material model, the implementation of a strain-based formulation and stress integrations for moment calculations.
- The OpenSees adjustments needed to develop a framework that includes uncertainty in material properties at elevated temperatures are discussed to achieve the third objective.

Validation studies and examples are provided to illustrate the performance of the modified code. The modifications enhance the capabilities of the thermal module in OpenSees. The outcome is a program that can be used to efficiently perform back-to-back seismic and thermal analyses, with a seamless transition, to investigate FFE problems. In addition, the program can be used to incorporate reliability analysis in an enhanced thermal module or FEE study. A programming environment with such capacities has not been available to the civil engineering community, and this paper provides a step toward developing methodologies and tools for probabilistic analysis of structures under multi-hazard scenarios.

2. OpenSees modifications

The thermal finite element code in OpenSees has three main phases [23]:

(1) Predictor: an initial out of balance force (due to external and thermal loads) is predicted, and used to calculate the corresponding displacement increment based on the stiffness matrix. The thermal load is treated as an element load which is then converted to equivalent nodal loads in a finite element formulation. Integrating the stresses in the fibers of a cross section results in section forces which represent the thermally induced element forces.
(2) Corrector: the displacement increment from the predictor is used to calculate the new total strain. The thermal strain is subtracted from the total strain to obtain the mechanical strain, which is then used to solve for the stress state. Integration of stresses over the cross section provides the out of balance force. The procedure is iterative and follows the general analysis procedure in OpenSees.
(3) Convergence check: out of balance forces are checked and convergence is achieved when the structure is in equilibrium. This step follows the established procedures in the original OpenSees.

This section discusses the modifications applied to the thermal module. The modifications include the constitutive material model of steel for mechanical stress calculations in the corrector phase and resultant moment calculations as part of the stress integration in the predictor phase. The proposed changes are validated in Sections 3 and 4.

2.1. Constitutive material model

The code modifications that are discussed in this paper are all applied to the Material Class of the source code. Fig. 1 shows the structure of the material class in OpenSees, as well as the classes that are added or modified as part of the new thermal module [23]. The three material classes added for steel structures under fire include *SteelECThermal*, *Steel01Thermal*, and *Steel02Thermal*. *SteelECThermal* was added to the OpenSees source code recently and was developed based on the Eurocode stress–strain relationship, including the divergence of the proportional limit from the yield strength [38]. However, the material model is not designed to handle the cyclic nonlinear response of steel material due to seismic loads.

Steel01Thermal and *Steel02Thermal* were developed based on the existing *Steel01* and *Steel02* classes respectively, and are therefore capable of handling cyclic seismic load. The two thermal classes were created as a temperature dependent material class with a bilinear stress–strain relationship, and with thermal properties based on the Eurocode formulation. This section discusses modifications to the constitutive material model in the *Steel01Thermal* class, but the changes can be extended to other classes such as *Steel02Thermal*.

The constitutive material model in *Steel01Thermal* is currently programmed with the following two assumptions:

(1) A bilinear elastic perfectly plastic material model at elevated temperatures, and
(2) A stress-based formulation (as opposed to strain-based) which cannot accommodate a strain reversal.

The first assumption could be taken as a simplification; however, it is widely accepted that the elastic perfectly plastic stress strain relationship at ambient temperatures transitions to a non-linear relationship at elevated temperatures. According to the Eurocode formulation [6], the yield stress (σ_y) is equal to the yield stress at ambient temperatures ($\sigma_{y,20}$) multiplied by $k_{y,T}$, a yield stress reduction factor that becomes less than 1.0 when temperatures exceed 400 °C. Similarly, the reduction factor $k_{E,T}$ for the modulus of elasticity (E) becomes less than 1.0 when temperatures exceed 100 °C. Finally, the proportional limit stress (σ_p) no longer equals to the yield stress (σ_y) at higher temperatures, and the stress–strain relationship becomes non-linear, as shown in Fig. 2a. As a simplification, Quiel and Garlock [26] previously

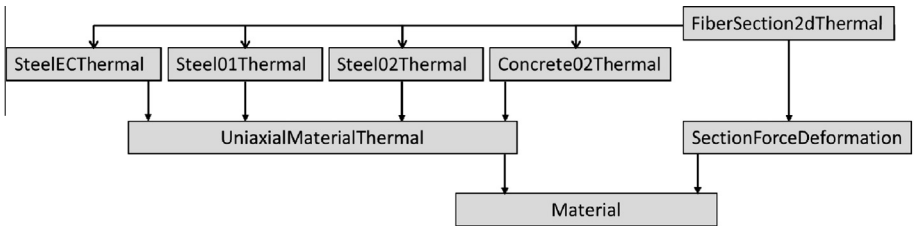

Fig. 1. Modified or added classes to the material class in the thermal module of OpenSees (adopted from Jiang et al. [22]).

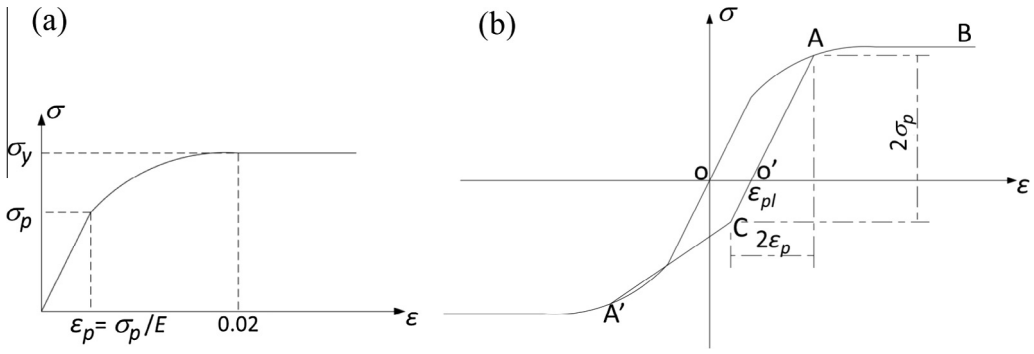

Fig. 2. Material model for steel at high temperatures (a) stress–strain model [6] (b) plastic strain and strain reversals.

implemented a simplified tri-linear model (the points of proportional limit and yield are linearly connected) in which plastic strain is used to define the stress–strain relationship. In this paper, the *Steel01Thermal* material class in OpenSees is modified such that the nonlinearity between the points of proportional limit and yield are fully coded with no simplification.

The implication of the second assumption is that the program is only able to start thermal analysis from a state of zero strain (which would not be the case in a FFE scenario). In addition, performance of the structure during cooling may not be correctly captured since strain reversals are not considered. During a building fire, it is likely that the elastic limit will be exceeded and plastic deformations will develop as a result of the reduction in the stiffness and strength of steel at elevated temperatures. This material softening can be modeled using a set of stress–strain plots (similar to Fig. 2a) which only depend on temperature. This holds true during heating, but when strain reversals occur in sections which exceeded the elastic limit, the material unloads elastically and the stress–strain relationship can no longer be defined using only the temperature [13,11].

Previous studies by Franssen [13] and El-Rimawi et al. [11] showed that the plastic strain rather than the maximum stress level should be used to describe the complete stress–strain history as the steel temperature changes during heating or cooling. The fundamental assumption of the applied formulation is that, at any point during heating or cooling, the full stress–strain curve can be constructed by knowing the plastic strain (point O' in Fig. 2b) and the elastic modulus for the given temperature [13,11]. In Fig. 2b, OAB is the path that the material would take starting from a zero strain. However, plastic strain develops in the steel material when it is loaded beyond its proportional limit. If the plastic strain is calculated to be at point O', a new full stress–strain path should be constructed. Point A is the intersection of path OAB and the line extending from O' with slope E. During the cooling phase, Point C can be found knowing that the length of linear portion is always the same ($2\sigma p$ and $2\varepsilon_p$). Finally point A' is the mirror of point A with respect to the origin. More detail regarding the inclusion of the plastic strain in the constitutive material model at elevated temperatures is provided by Franssen [13], El-Rimawi et al. [11], and Quiel and Garlock [26].

Fig. 3a shows the constitutive material model for two consecutive time steps with increasing temperatures in the original thermal module. The constitutive model incorporates the reduction in yield strength and modulus of elasticity due to a temperature increase from time step (i) to ($i+1$). Given the strain increment $\Delta\varepsilon$, the state of the material moves from point A_o with temperature $T(i)$ to point B_o with temperature $T(i+1)$. If the effect of proportional limit were included, points A and B would have been the state of material at time steps (i) and ($i+1$). The transition from time step (i) to ($i+1$) is achieved by preserving the mechanical strain from the end of step (i) to the beginning of step ($i+1$) – this is performed graphically by tracing vertically down from point A (or A_o) on the material model at step (i) to point C, which lies on the stress–strain curve for step ($i+1$). The tangent modulus for the first iteration of analysis at time step ($i+1$) is calculated at point C, and the iterations progress until equilibrium is obtained for the strain increment $\Delta\varepsilon$ at point B (or B_o).

Fig. 3b shows the material model for the same two time steps while incorporating the modifications. Having converged at time step (i) (with temperature $T(i)$, strain $\varepsilon_{(i)}$, stress $\sigma_{(i)}$, and modulus of elasticity $E_{(i)}$), the plastic strain $\varepsilon_{pl(i)}$ is calculated by "unloading" from point A with slope $E_{(i)}$ to the intercept with strain axis. The temperature then increases at step ($i+1$), and a new stress–strain curve considering the reduced yield strength, proportional limit, and modulus of elasticity is constructed. The plastic strain $\varepsilon_{pl(i)}$ and the material model shown in Fig. 2b are used to construct the new stress–strain path that the material takes at time step ($i+1$). Prior to the first iteration at step ($i+1$), the material is "reloaded" from the strain axis intercept at $\varepsilon_{pl(i)}$ via slope $E_{(i+1)}$ to point C, which has the same mechanical strain as point A from the end of time step (i) [11]. Both the plastic strain and the mechanical strain at point A, which together characterize the physical state of the material at the end of step (i), are therefore preserved during the transition to the beginning of step ($i+1$). The tangent modulus for the first iteration of analysis at step ($i+1$) is calculated at point C, and the iterations progress until convergence

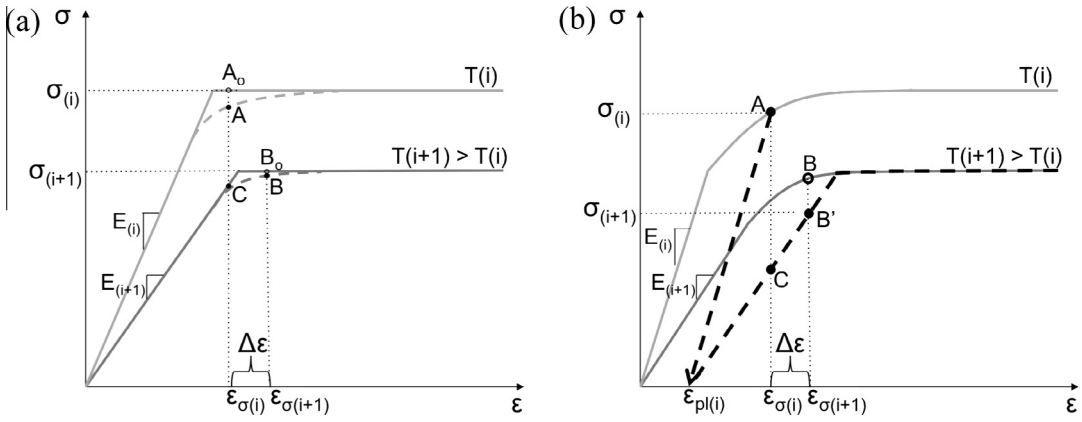

Fig. 3. Constitutive material model (a) original OpenSees (b) modified.

for the force-balance solution is obtained for a strain increment of $\Delta\varepsilon$ at point B', which lies on the updated and modified stress–strain pathway for step $(i+1)$. If the preservation of plastic strain between time steps were neglected as was done in Fig. 3a, then point B in Fig. 3b would have been the state of material at step $(i+1)$.

The above process involves two major considerations for advancing the time steps while temperature is changing: (1) plastic strain is calculated at the beginning of every time step and is used in conjunction with mechanical strain as the tracer between time steps; and (2) the updated stress–strain path at each time step (i.e. at each temperature change) is constructed based on material properties (yield strength, proportional limit, and modulus of elasticity) at the current temperature as well as the relative location of the proportional limit and plastic strain. The process applies to both cooling and heating phases of a fire scenario.

2.2. Resultant moment

The *Steel01Thermal* material class returns stress values based on the coded constitutive material model. Axial load and moment values are calculated by stress integration along the fibers in the cross section in the *FiberSection2dThermal* function that was shown in Fig. 1. In the original OpenSees approach (seismic module), the reference axis for calculating the moment is taken as the geometric centroid of the cross section. This section discusses the current formulation in the thermal module for moment calculation, and proposes a change in the way internal moments are calculated. Both the original and modified codes will be used in an example problem, and the proposed modification will be validated.

Jiang and Usmani [23] explain that for the thermo-mechanical analysis in the new module of OpenSees, the unbalance force (F_u) in the finite element formulation should include the thermal forces and material softening:

$$F_u = F_{ex} + F_{th} - F'_{re} \tag{1}$$

where F_{ex} is the external load including nodal load and element load; F_{th} is the thermal load; and F'_{re} is the updated resisting force due to material softening. The thermal load F_{th}, is a matrix of thermal axial load and thermal moment in the cross section, calculated by:

$$F_{th} = \left[\bar{F}\ \bar{M}\right] = \left[\sum_r F_r = \sum_r E_r A_r(\varepsilon_{th})_r \quad \sum_r F_r(z_r - \bar{z})\right] \tag{2}$$

Subscript "r" in the moment calculation in Eq. (2) represents a given fiber in a cross section. z_r is the location of fiber r, and $\bar{z}$ is the centroid of the cross section [23]. In the current version of OpenSees, the centroid of the section $\bar{z}$ (in Eq. (2)), is calculated based on the following expression:

$$\bar{z} = \frac{\sum_r A_r E_r z_r}{\sum_r A_r E_r} \tag{3}$$

Since the modulus of elasticity of each fiber, E_r, is included in $\bar{z}$, the calculated centroid in Eq. (3) takes the effect of thermal gradient into account and calculates the *effective centroid* (i.e. the center of stiffness). Therefore, in Eq. (2), the moment is calculated with respect to the *effective centroid* and not the geometric centroid. When a thermal gradient is present, the effective centroid is not necessarily equal to the geometric centroid [16]. This has been modified by the authors to ensure that moment is calculated in the thermal module with respect to the geometric centroid, as shown in Eq. (4):

$$\bar{z} = \frac{\sum_r A_r z_r}{\sum_r A_r} \tag{4}$$

3. Validation studies of modified OpenSees

This section provides two validation studies, one for a single element and the other using frame examples. The results from the modified OpenSees module (OS_ModifiedThermal) and the original thermal module in OpenSees (OS_OriginalThermal) are compared with results from test data and/or finite element modeling results obtained using SAFIR, a software developed at the University of Liege specifically for the analysis of structures under fire [14]. SAFIR performs uncoupled analyses of, first, a thermal model of each member exposed to fire and, second, a structural model of the frame composed of those members. The first validation study examines the performance of a single perimeter column that develops a thermal gradient through its depth due to non-uniform fire exposure, as presented in a previous study by Quiel and Garlock [27]. This study demonstrates the ability of OS_ModifiedThermal to model the structural effects of the thermal gradient, particularly the aforementioned influence of geometric and effective centroids on moment calculations, via comparison with computational results from OS_OriginalThermal and SAFIR. The second study is based on two steel frames that were previously selected by Jiang and Usmani [23] for validation of the original thermal module in OpenSees. The two steel frames, labeled EHR3 and ZSR1, are based on a series of experimental tests performed in Germany in 1980s [31,32]. This study compares the computational results from OS_ModifiedThermal and SAFIR with the previously published test results to validate the ability of the modified

code to model the response of a steel frame to elevated temperature.

3.1. Single element validation: 1MP perimeter column

The first validation example involves a W14 × 314 steel perimeter column (Fig. 4) that is exposed to three-sided fire, thus producing a thermal gradient through its depth along the strong axis. It is assumed that there is no fire protection on the member. The column is 3.56 meters in height, and is assumed to be fixed at the bottom and restrained from rotation at the top (i.e. the top of the column is unrestrained to vertical translation). The prototype column represents an actual perimeter column from steel building frame of the One Meridian Plaza (1MP), formerly of Philadelphia, PA, with $F_{y,20}$ = 250 MPa, and P/P_y = 25% [27]. The applied fire temperature–time curve is based on the actual 1MP fire event [15], and the resulting steel temperatures for the web and two flanges due to fire exposure are obtained from the previous study by Quiel and Garlock [27] and are shown in Fig. 5.

In response to the thermal gradient, two moment reactions develop in the column due to (1) restraint of thermal bowing due to temperature variation in the cross section, and (2) the shift in center of stiffness (effective centroid). Regarding the second moment reaction, the reduced modulus of elasticity at elevated temperatures becomes non-uniform in the cross section due to the thermal gradient. Therefore, the effective centroid shifts toward the cooler side. The axial load P, applied at the geometric centroid (which no longer coincides with the effective centroid), generates an eccentric moment equal to P times the distance between the effective and geometric centroids. These reactions create opposing bending moments that heavily contribute to the column's fire-induced response [16].

The 1MP column is modeled in OpenSees with 8 *dispbeamcolumnThermal* elements. Each element is made of three sections and each section consists of fibers. The W14 × 314 cross section is modeled with 4 fibers in each flange and 8 fibers in the web. The *Steel01Thermal* material class is assigned to all the elements. In SAFIR, the length of each column is modeled using 8 three-noded 2-D non-torsional fiber-beam elements. The W14 × 314 cross section is again modeled with 4 fibers in each flange and 8 fibers in the web, and the *STEELEC3* material model is assigned to all elements. Both the OpenSees and SAFIR models implement the Eurocode 3 material model for steel at elevated temperatures [6].

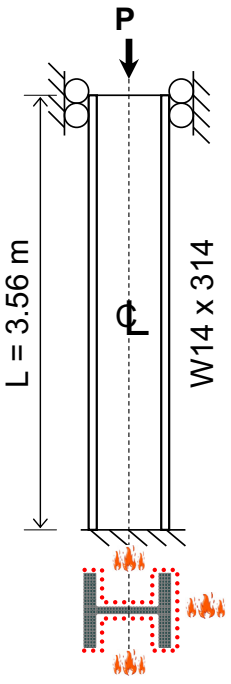

Fig. 4. 1MP perimeter column.

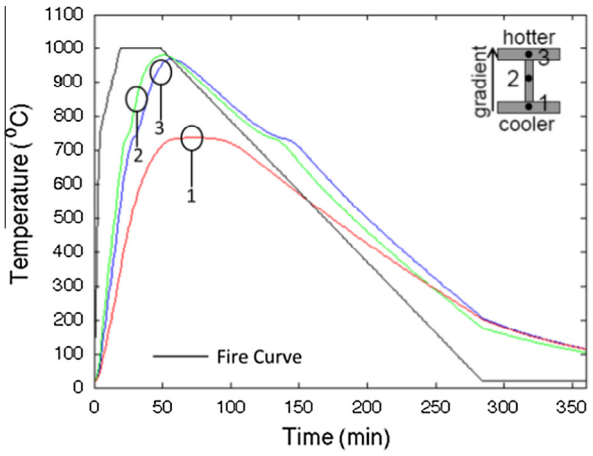

Fig. 5. Fire and steel cross-sectional time–temperature curves.

The column is analyzed using (1) the original OpenSees code (OS_OriginalThermal), (2) the original OpenSees with modified constitutive material model as described in Section 2.1 (OS_NewMaterial), (3) the original OpenSees with modified material (Section 2.1) and modified moment calculation as described in Section 2.2 (OS_ModifiedThermal), and (4) SAFIR.

Fig. 6(a) shows the normalized P–M path that the column takes until failure for OS_OriginalThermal and OS_NewMaterial. The plot compares those curves with the normalized P–M path calculated by SAFIR and the plastic P–M interaction capacity envelope at the time of failure calculated based on Garlock and Quiel [17]. The plot shows that the normalized P–M path steps outside of the capacity envelope when calculated using the current formulation in OpenSees, and with the module with the updated material model but no change in the moment calculation. P–M points outside the envelope are not physically possible since the envelope represents the plastic capacity of the section. However, when the reference axis for moment calculation is changed to the geometric centroid, Fig. 6(b) shows that the P–M path always stays inside the envelope and reaches the envelope at 34 min, at which time the analysis stops converging. SAFIR results follow essentially the same path and predict that the column reaches plastic hinge only one minute sooner than OS_ModifiedThermal version of OpenSees (at 33 min).

Fig. 7 compares cross sectional moment values over time, calculated using SAFIR and the three versions of the OpenSees thermal module. The initial increase in moment is caused by the restraint of thermal bowing and is captured by all four analyses. It is shown that the modification in the *Steel01Thermal* code (OS_NewMaterial) improves the accuracy versus the OS_OriginalThermal module in the period between 10 and 20 min. The earlier moment reversal in OS_NewMaterial, OS_ModifiedThermal, and SAFIR is caused by the accumulation of inelastic plastic strains in the hotter flange due to the use of the nonlinear material model for heated steel. In contrast, the OS_OriginalThermal module does not include this nonlinearity and allows the moment due to the restraint of thermal bowing to increase for a longer period until the elastic-perfectly-plastic material begins to yield. After 20 min, the temperature in the hotter flange and the web are around 600 °C while the temperature in the cooler flange is still under 400 °C (see Fig. 5).

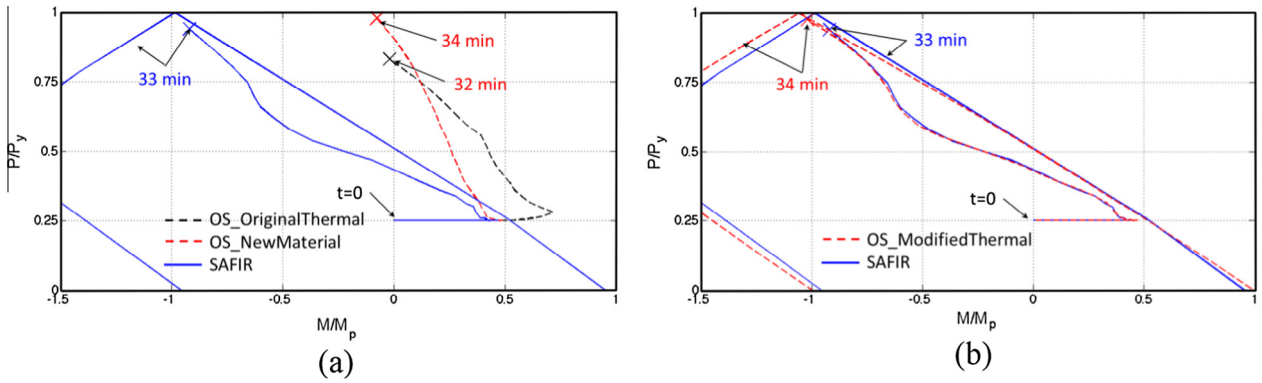

Fig. 6. Comparison of normalized *P–M* plots from SAFIR with (a) OS_OriginalThermal and OS_NewMaterial, and (b) OS_ModifiedThermal.

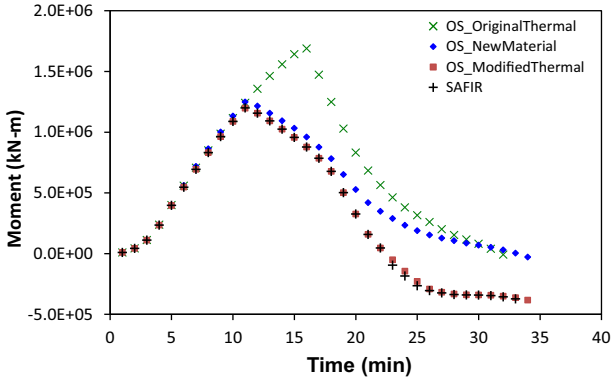

Fig. 7. Comparison of moments calculated by SAFIR and OpenSees.

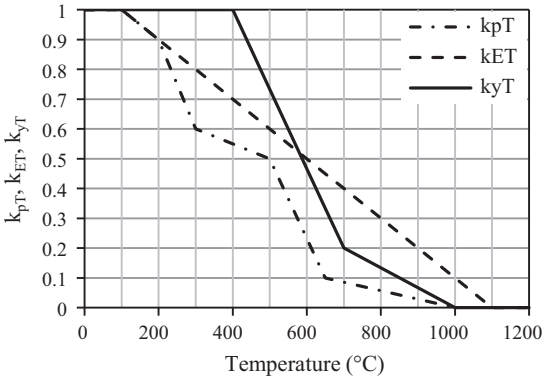

Fig. 9. Material properties of St 37 at elevated temperatures [32].

Therefore, the effective centroid starts to distance considerably from the geometric centroid. By modifying the moment calculation, OS_ModifiedThermal results are in good agreement with the SAFIR prediction.

3.2. Frame validation: EHR3 and ZSR1

Fig. 8 shows the two steel frames, EHR3 and ZSR1, and the applied loads on each. Both frames were composed of IPE80 I-shaped sections with St 37 steel grade [32]. The modulus of elasticity at ambient temperature for both frames was 210,000 MPa; the ambient yield strength for the EHR3 and ZSR1 frames was 382 MPa and 355 MPa, respectively [32]. The material properties of St 37 at elevated temperatures are shown in Fig. 9 – note that this material model is similar but has some variation compared to that of Eurocode 3 [6]. All boundary conditions shown in Fig. 8 are pinned.

Each frame is modeled in both OpenSees and SAFIR with four elements in each column and in each beam length between supports. The I-beam section is modeled with eight fibers in the web and four fibers in each flange. In addition to the externally applied point loads shown in Fig. 8, the dead weight of the beam is represented as a uniformly distributed load of 60 N/m.

During the experiments, uniform heating was applied as indicated in Fig. 8 until failure due to loss of stability. Figs. 10 and 11 show the displacements recorded during the experimental tests of both EHR3 and ZSR1 at the locations indicated in Fig. 8 [31]. The plots in both figures show close agreement between the test data and displacements calculated via SAFIR and the modified OpenSees module OS_ModifiedThermal.

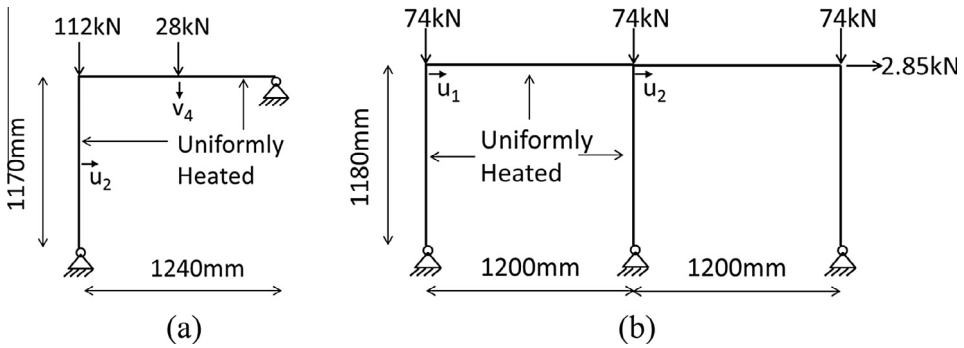

Fig. 8. Configuration of validation frames [32]: (a) EHR3 and (b) ZSR1.

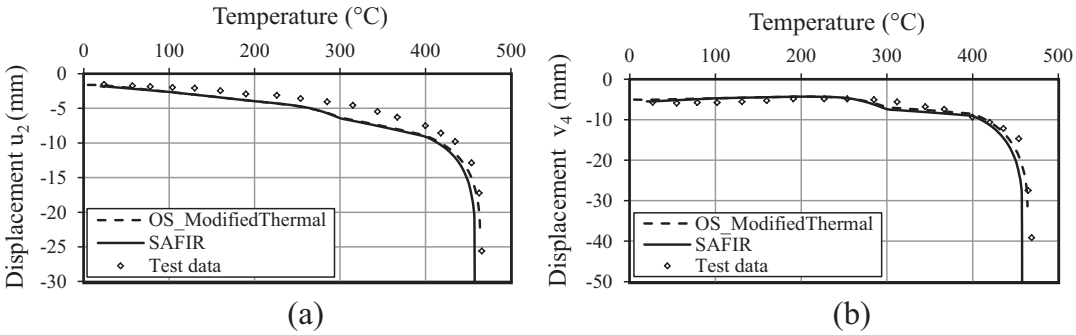

Fig. 10. Comparison of EHR3 experimental displacements with OS_ModifiedThermal and SAFIR: u_2 and v_4.

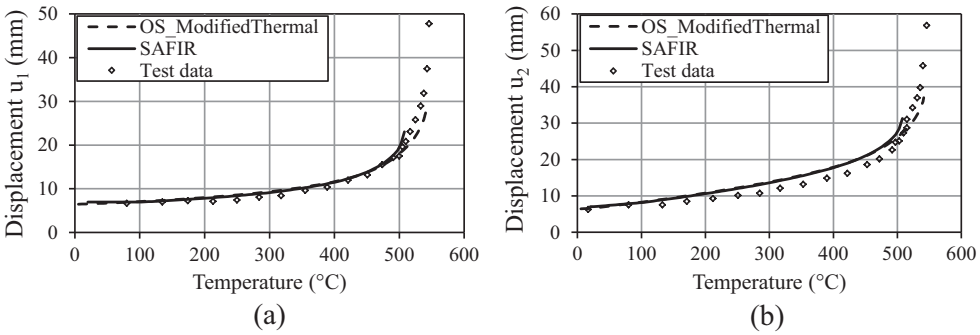

Fig. 11. Comparison of ZSR1 experimental displacements with OS_ModifiedThermal and SAFIR: u_1 and u_2.

4. Multi-hazard OpenSees analysis for a multi-story frame

In Section 3, the new code was validated for thermal analysis in simple members or frames. In this section, the modified OpenSees code is used to evaluate the performance of a 9-story steel building for fire following earthquake (FFE) scenarios. These analyses demonstrate the ability of the new code to perform seamless, sequential analysis of seismic and subsequent thermal effects.

The procedure to evaluate post-earthquake fire performance of a frame is as follows:

(1) Select an earthquake scenario (i.e. develop the load input for seismic analysis).
   a. Select a design-basis ground motion or equivalent lateral forces.
(2) Select a fire scenario (i.e. develop the load input for structural-fire analysis).
   a. Select a compartment location within the frame.
   b. Define a fire scenario with the full temperature–time curve.
   c. Perform heat transfer analysis to develop temperature–time curves for fire-exposed structural elements.
(3) Perform seismic structural analysis.
(4) Change model constraints to allow for thermal expansion.
(5) Perform structural-fire analysis.

The following sections describe the implementation of this procedure for the 9-story prototype frame and discuss the results for both fire-only and FFE scenarios.

4.1. Design description

The geometry and building description of the prototype Moment Resisting Frame (MRF) is based on the SAC steel project [33]. The SAC project includes 3, 9, and 20-story prototype buildings located in Los Angeles, Seattle and Boston. The buildings were designed as standard offices on both stiff and soft soil. The MRF in the present study is a 9-story frame that is located in downtown Los Angeles and has plan and elevations that are based on SAC buildings but considered only for stiff soil. The MRF is re-designed based on ASCE7-10 specifications [4].

The floor plan and elevation of the 9-story structure is presented in Fig. 12. The building geometry consists of a square plan with 5 bays, each at 30 ft. (9.14 m), in either direction. Girders are spaced at 30 ft. (9.14 m) and beams are spaced at 10 ft. (3.05 m) intervals. The 9-story building has a typical floor height of 13 ft. (3.96 m) with a basement height of 12 ft. (3.66 m) and ground floor height of 18 ft. (5.50 m) The building consists of 4 MRFs, one on each side, that are placed such that biaxial bending is avoided at corners. The MRFs in the two orthogonal directions are identical. The columns are pinned at the foundation, and laterally braced at the ground level.

The design procedure is primarily based on the ASCE7 specifications [4], and the assumed gravity loads are consistent with the assumptions of the SAC models [33]. Seismic loads are according to the Equivalent Lateral Force (ELF) procedure in ASCE7 [4]. The design forces are calculated for Site Class D (stiff soil). The design checks applied in the design of the MRF are based on the guidelines in the AISC Steel Construction Manual [1], and AISC Seismic Provisions for Structural Steel Buildings [2]. The frame has a period of 1.75 s. Table 1 summarizes design of the 9-story MRF.

4.2. Seismic modeling

Fig. 13 shows the analytical model for the 9-story frame in OpenSees. The nonlinear behavior of the 9-story building under dynamic loading is modeled via the concentrated plasticity concept by using rotational springs. The frame is modeled with elastic beam-column elements that are connected with zero-length

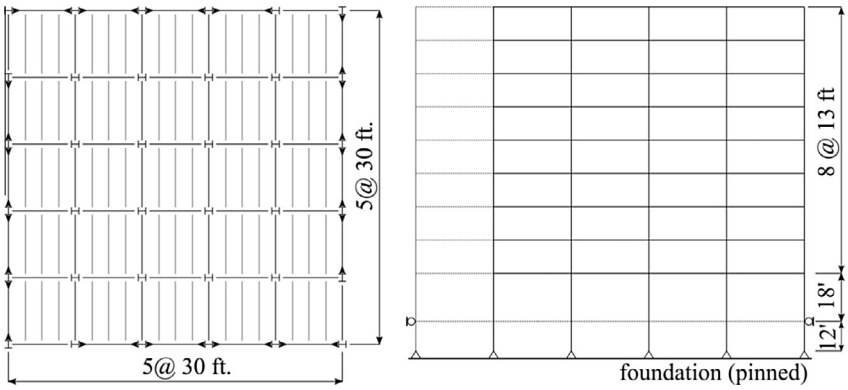

Fig. 12. Plan and elevation of the 9-story frame.

Table 1
Design of the 9-story frame based on ASCE 7-10.

Level	Beam	Interior column	Interior tdoubler[a] in. (cm)	Exterior column	Exterior tdoubler[a]
9-roof	W24 × 76	W14 × 342	0.00 (0.00)	W14 × 257	0.00
8–9	W30 × 108	W14 × 342	0.47 (1.20)	W14 × 257	0.00
7–8	W33 × 169	W14 × 455	0.92 (2.34)	W14 × 370	0.00
6–7	W33 × 169	W14 × 455	0.92 (2.34)	W14 × 370	0.00
5–6	W36 × 194	W14 × 550	0.70 (1.78)	W14 × 500	0.00
4–5	W36 × 194	W14 × 550	0.70 (1.78)	W14 × 500	0.00
3–4	W36 × 194	W14 × 605	0.38 (0.96)	W14 × 550	0.00
2–3	W36 × 210	W14 × 605	0.63 (1.60)	W14 × 550	0.00
1–2	W36 × 210	W14 × 665	0.45 (1.14)	W14 × 605	0.00
Basement-1	W36 × 210	W14 × 665	0.45 (1.14)	W14 × 605	0.00

[a] Thickness of column web doubler plate in the panel zone area.

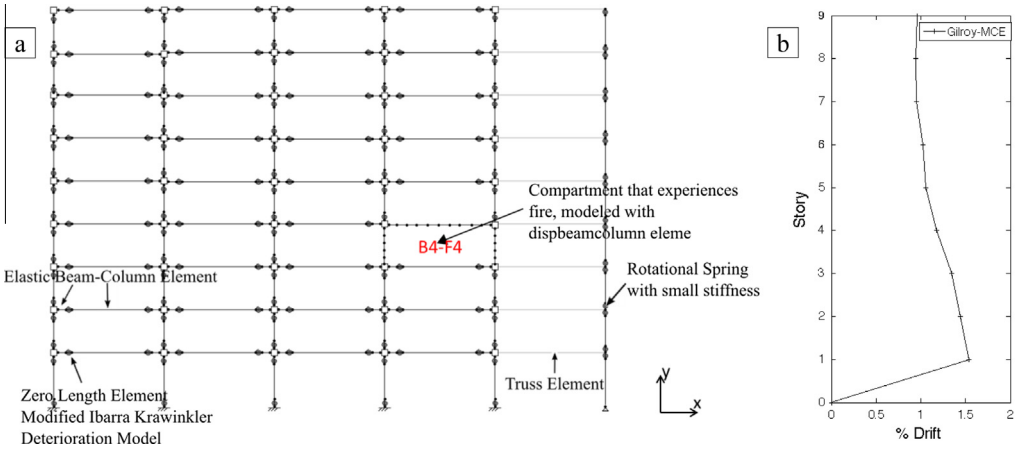

Fig. 13. Analytical OpenSees model for seismic and thermal analysis: (a) elevation and (b) % drift at the end of earthquake.

elements. The zero-length elements serve as the rotational springs that follow a bilinear hysteretic response based on Modified Ibarra Krawinkler Deterioration Model [24,20,29]. When subjected to seismic excitations, plastic hinges are formed in beams at an offset from the beam-column joints. The offset can be estimated as 1/3rd of the beam depth from the column edge according to [12]. Panel zones are also modeled to capture the shear distortion in beam-column joints [19]. Therefore, rotational springs are placed at a distance of 1/3rd of the beam depth from the panel zone edge.

A leaning-column that carries gravity load is linked to the frame to simulate P-Delta effects. The leaning-column is modeled with elastic beam-column elements with large cross-sectional area and moment of inertia to capture the effect of the gravity columns on the overall response of the frame. The beam-column elements are linked by rotational springs with very small rotational stiffness. This ensures that the leaning-column does not capture significant moment. Finally, the leaning column is connected to the frame by truss elements that are axially rigid.

4.3. Thermal modeling

To efficiently perform a post-earthquake fire analysis, the procedure must seamlessly transition from seismic to thermal in the OpenSees environment. However, thermal modeling in OpenSees is only possible with *dispBeamColumnThermal* type element [23], while the seismic model discussed in Section 4.2 uses various other element types, including zero-length deterioration spring elements to capture nonlinear behavior. The approach in this study is to

model the 9-story frame using the seismic modeling with the springs, except for the beams and columns that are assumed to be heated in a fire (which will be modeled with *dispBeamColumnThermal* elements) as shown in Fig. 13. The *dispBeamColumnThermal* element is defined using fibers and considers plasticity along its length. The number of fibers in the cross section was selected to optimize efficiency without compromising accuracy. The thermal element is modeled using 8 fibers in the web, and 4 fibers in each flange. The element requires temperature inputs through the depth of the cross section, the calculation of which OpenSees is not currently capable. The temperature is defined using 9 temperature points (8 layers) through the depth and steel time–temperature curves.

4.4. Transition from seismic to thermal

Modification of the model is necessary when transferring from the seismic to the thermal analysis. During the seismic analysis, a constraint is placed on the nodes of every floor to ensure that they move together horizontally, representing the effect of concrete slab in the composite structure. However, a previous study by Quiel and Garlock [28] shows that, during the thermal analysis, steel in the composite girder experiences a faster increase in temperature than the slab. The steel expands at a faster rate than concrete, which eventually results in cracking of concrete, thus rendering the slab negligible for axial restraint. Therefore, after the seismic analysis is completed, the constraint on the nodes of the compartment that would experience fire is removed. It should be noted that Quiel and Garlock [28] shows that the slab has a considerable effect on the thermal analysis of the composite girder and the temperature of the top flange, which will be discussed later.

4.5. Ground motion selection

The ground motion used in this study will be referred to as "Gilroy" ground motion, which represents the 1989 Loma Prieta, CA earthquake ground motion that was recorded at station 47381 Gilroy (Array #3). Only one component of the ground motion (the G03090 component) is applied since two-dimensional models are being used. The location was on stiff soil, and the earthquake had a magnitude of 6.9 with the closest distance from a fault rupture zone of 14.4 km. The hazard level chosen for this study is the Maximum Considered Earthquake (MCE). The selected ground motion is first scaled to a level compatible with the 5% damped ASCE 7-10 design spectrum (the design basis earthquake). The design basis earthquake scale is then multiplied by 1.5 to obtain the required scale for the MCE level. The scaling procedure is based on the work of Somerville et al. [37], where the scale factor minimizes the squared error between the ASCE 7-10 target spectrum and the response spectrum of the natural ground motion assuming a lognormal distribution of amplitudes. The scale factor for the Gilroy ground motion is calculated to be 2.78 for the MCE level.

4.6. Fire load and heat transfer

The fire temperature–time history for this study is based on the aforementioned 1MP fire curve [15], which is representative of an actual fire event. This study assumes a single compartment with dimensions of 20 ft. (6.1 m) wide by 30 ft. (9.1 m) deep. Given that the fire occurs after an earthquake, it is assumed that the compartment has *no* functional active fire-fighting measures and the passive fire protection (e.g. spray) has been damaged enough to render it ineffective. The heat transfer analysis is performed to obtain steel temperatures for the beam, perimeter column and interior column of the location shown in Fig. 13. Heat transfer for the two columns and a beam in the fire compartment is based on the closed-form solution developed by Quiel and Garlock [27], which represents the steel cross-section using multiple lumped masses. For the beam, the solution is modified to include the effect of concrete slab (which acts as a heat-sink) on the top flange temperature. An empirical equation developed by Ghojel and Wong [18] is used to calculate the heat transfer between the top flange and the slab. Fig. 14 shows the fire curve and weighted average steel temperature–time curves for beams and columns at the B4–F4 location shown in Fig. 13.

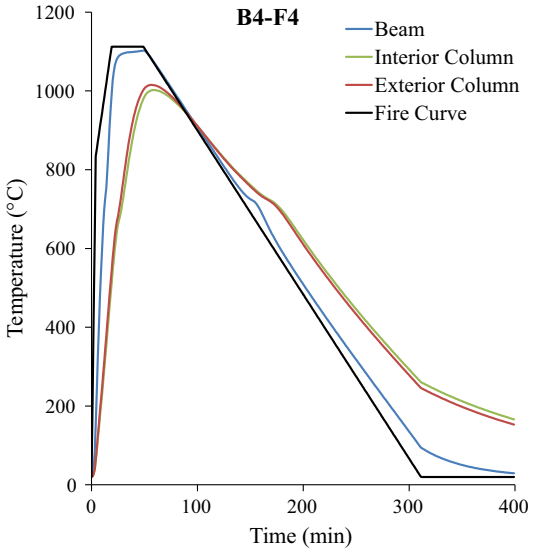

Fig. 14. Temperature–time plots for fire curve and steel (weighted average).

4.7. Results

Results for the B4–F4 compartment are summarized in this section. The analyses are performed for (1) fire-only, and (2) fire after the MCE level earthquake. Section 3 provided validation for fire-only scenarios. This section will first highlight enhancements to the OpenSees code via a comparison of OpenSees results for fire after the MCE earthquake from the original thermal module (OS_OriginalThermal) and the modified version (OS_ModifiedThermal). The rest of this section will focus solely on results from the modified version.

Fig. 15a shows strain values during the earthquake at the lowest fiber in the web of the beam located at the beam and exterior column joint. For the same fiber, Fig. 15b shows mechanical strain values during the fire that develops after the earthquake. During fire, the total strain in every fiber is comprised of mechanical strain and thermal strain (which equals to the coefficient of thermal expansion times the change in fiber's temperature) [27]. The total strain is calculated based on the fundamental assumption of plane sections remaining plane. The mechanical strain is the difference between the total and the thermal strains for every time step. The mechanical strain is then used within the constitutive material model to calculate stress in each fiber.

Fig. 15a shows that the strain values during earthquake are identical for both OpenSees versions. However, Fig. 15b shows that strain in the OS_OriginalThermal version plunges almost instantaneously to a value of −20 mm/mm about 15 min after the fire starts and then flat-lines for the remainder of the analysis. This precipitous drop is a non-physical result and indicates premature numerical "failure." The strain values from OS_ModifiedThermal version are physically reasonable and confirm yielding of the fiber

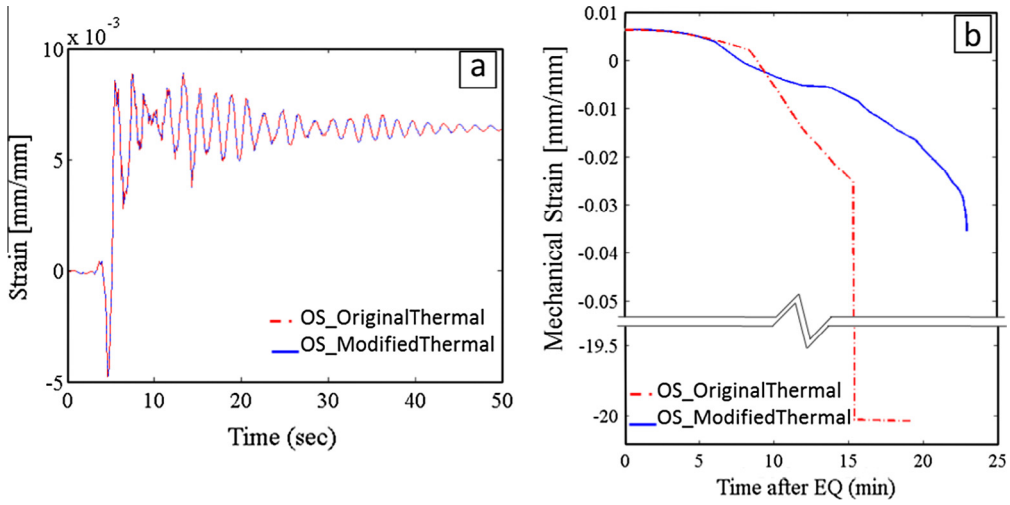

Fig. 15. Comparison of original and modified OpenSees versions for the 9-story frame during (a) MCE earthquake, and (b) the fire that follows the earthquake.

at the time that the analysis ends. This difference in strains from the two versions of OpenSees is due to the differences in the constitutive material model as described previously in Section 2.1.

Fig. 16 shows the normalized *P–M* (axial load-moment) path of the beam at the right and left interfaces with the columns, and at the beam mid-span. The paths are shown in relation to the normalized plastic *P–M* capacity envelopes at time zero and failure. The *P–M* paths for the left and right ends of the beam reach the *P–M* capacity envelope first. However, the beam does not fail until a third plastic hinge forms at mid-span. At this point, three plastic hinges are formed at three locations in the beam. It should be noted that the capacity envelopes are drawn for the first and last time steps only. The capacity envelope changes shape with time as the thermal gradient in the cross section changes. All the *P–M* paths, shown in Fig. 16, that are outside of the two drawn envelopes were inside the capacity envelope at the relevant time.

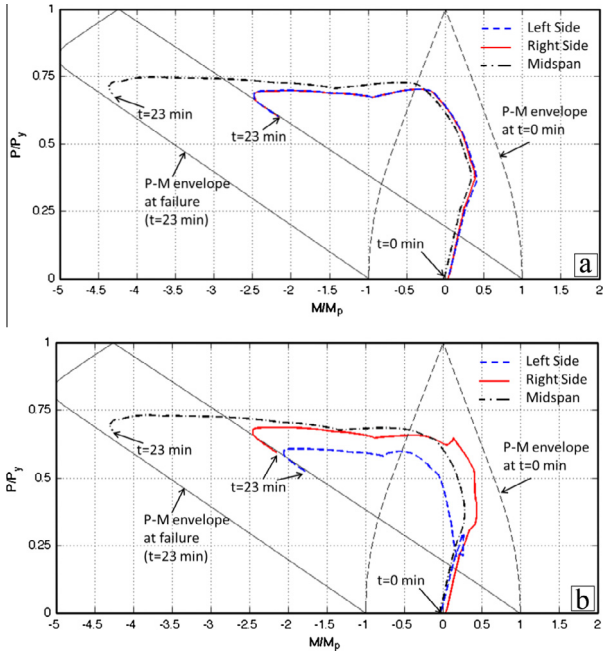

Fig. 16. Normalized *P–M* interaction for the beam in B4–F4 under (a) fire-only and (b) fire following the MCE EQ.

Fig. 17 shows the deflection at the beam mid-span and the pseudo-velocity (i.e. the rate of change in vertical displacement [cm/s]) of the beam and the perimeter column. It can be seen that when the third plastic hinge forms at the beam mid-span, the pseudo-velocity of the beam drops sharply, indicating loss of stability in the beam. The analysis stops converging at this point, indicating beam "failure."

The results for both cases of fire-only and fire that follows the MCE earthquake are similar. Table 2 summarizes results for the two loading scenarios. The following parameters are recorded and presented in the table: (1) the time (from the start of the fire) to form a plastic hinge at the interface of the beam and perimeter column t_{pR}; (2) the time (from the start of the fire) to form a plastic hinge at the interface of the beam and interior column t_{pL}; (3) the time (from the start of the fire) to form a plastic hinge at the beam mid-span t_{pM}; (4) the maximum and residual drift after the earthquake, thus representing the initial condition before the fire; (5) the maximum and residual drift at the end of fire or fire that follows earthquake.

Comparison of results for the fire-only and the post-earthquake fire scenario indicates the following:

(1) The earthquake slightly decreases the time to form a plastic hinge at the interface of beam and the perimeter column, while increases the time at the interface of beam and the interior column. This is mainly due to presence of locked-in moments in the beam after the earthquake, and confirms that the modified code captures the effect of earthquake on the thermal behavior of the beam.

(2) Considerable column drifts, approaching 1.70%, are possible for fires that follow earthquake. During heating, the beam expands outwards, inducing positive drift in the perimeter column and negative drift in the interior column (positive indicates positive *x*-direction shown in Fig. 13). This implies that fire adds to the earthquake-induced drift for the perimeter column and decreases the earthquake-induced drift for the interior column. These results are not generally conclusive of fire following earthquake response for tall steel buildings; however, these results show that the modified OpenSees modules are now capable of seamlessly analyzing fire following earthquake.

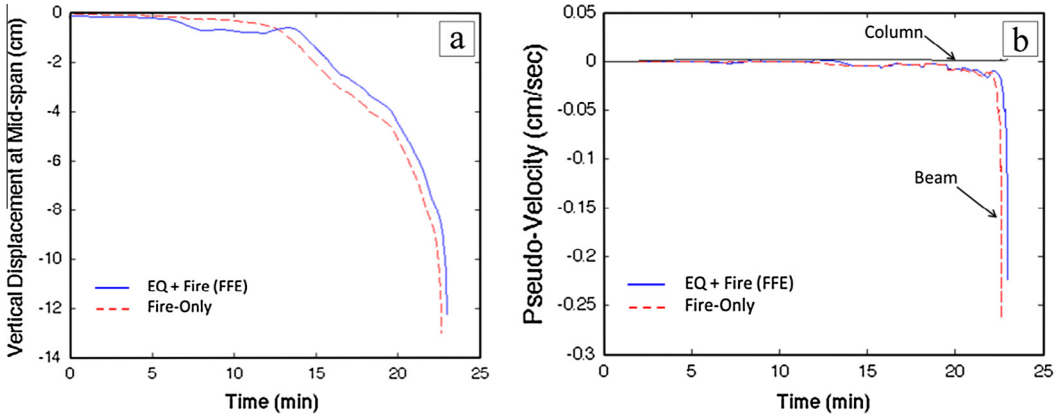

Fig. 17. Analysis results: (a) vertical displacement at the beam mid-span, and (b) vertical pseudo-velocity for the beam mid-span and the perimeter column at its beam interface.

Table 2
Summary of results for fire-only and fire following the MCE earthquake.

	Time to form plastic hinge (min)			Max vertical displacement (cm)	Drift (%)			
					EQ		Fire	
	t_{pR}	t_{pL}	t_{pM}		Max	Residual	Max	Residual
Fire-only	17	17	23	12.95	–	–	0.45	0.36
FFE (MCE)	15	20	23	12.24	2.71	1.22	1.70	1.65

5. Reliability module in OpenSees

5.1. Existing module

As a platform that was originally developed for computationally efficient seismic analysis, OpenSees has the capacity to be used in performance-based earthquake engineering. Therefore, it was of interest to the OpenSees developers to offer the program as a platform to perform nonlinear finite element analysis in the presence of uncertainties [36]. Previous attempts have been made to include a reliability module in OpenSees, but these efforts had resulted in an inflexible module that was difficult to work with [36]. However, the structure of the reliability module in the source code has been recently modified and updated such that it provides a flexible framework for potential extensions of the code.

In this section, the new thermal module is adjusted to be compatible with the available reliability module in OpenSees, making it possible to use OpenSees to perform nonlinear finite element analysis at elevated temperatures in the presence of uncertainties. The reliability module uses a parameterization approach, which identifies and updates parameters that have uncertainties associated with them. This section demonstrates the required set up for performing Monte Carlo analysis. Three commands from the reliability module are used for the purpose of this work: (1) *randomVariable*, which creates random variable objects using mean values, standard deviations, and probability distributions; (2) *parameter*, which creates parameters to the properties of interest (such as yield strength); and (3) *addToParameter*, which maps these parameters to the model. A detailed description of these commands is provided by Scott and Haukaas [35].

5.2. Implementing reliability in structural-fire analysis

The main uncertainties to consider during structural-fire analysis are fire load density (demand), as well as steel yield strength (F_y) and modulus of elasticity (E) at elevated temperatures (capacity). Variation in fire load density can be considered by generating a number of temperature–time curves and running the analysis for a set of fire curves. The approach is similar to the procedure that considers the uncertainty in ground motions in seismic analysis, in which the model is analyzed for a set of selected ground motions. In order to consider uncertainties in material properties during the structural-fire analysis, the user should set up random variables and parameters in the "tcl script," calculate temperature-dependent material properties and update the parameters at each time-step.

In order for the reliability setup to work, the temperature dependent equations for F_y and E had to be removed from the *Steel01Thermal* material class, and the user script specifies and updates the variables in each time step. Two tcl subroutines can be written and called during the analysis. The first subroutine takes the time step as an input and returns the temperature for a particular fiber at that time. The second subroutine takes the temperature (output of the first subroutine) as an input, and returns random values for F_y and E at the given temperature. Probabilistic equations for F_y and E that are based on measured data and a Bayesian based formulation have already been developed [10]:

$$k_{y,2\%,T} = 1.7 \times \frac{e^{\left[logit\left(\hat{k}^{*}_{y,2\%,T}\right)+0.412-0.81\times10^{-3}T+0.58\times10^{-6}T^{1.9}+0.43\times\varepsilon\right]}}{e^{\left[logit\left(\hat{k}^{*}_{y,2\%,T}\right)+0.412-0.81\times10^{-3}T+0.58\times10^{-6}T^{1.9}+0.43\times\varepsilon\right]}+1} \quad (5)$$

$$k_{E,T} = 1.1 \times \frac{e^{\left(2.54-2.69\times10^{-3}\times T-2.83\times10^{-6}T^{2}+0.36\times\varepsilon\right)}}{e^{\left(2.54-2.69\times10^{-3}\times T-2.83\times10^{-6}T^{2}+0.36\times\varepsilon\right)}+1} \quad (6)$$

Eqs. (4) and (5) are sample probabilistic equations for steel mechanical properties, where $k_{y,2\%,T}$ and $k_{E,T}$ are normalized yield strength (at a strain equal to 2%) and modulus of elasticity at elevated temperatures, T is temperature in degrees Celsius, and ε is a random variable that follows normal standard distribution [10]. In Eq. (5), $\hat{k}^{*}_{y,2\%,T} = (\hat{k}_{y,2\%,T} + 10^{-6})/1.7$ where $\hat{k}_{y,2\%,T}$ is the normalized 2% yield

strength based on Eurocode 3 [6], and $logit(\hat{k}^*_{y,2\%,T}) = \ln\left(\frac{\hat{k}^*_{y,2\%,T}}{1-\hat{k}^*_{y,2\%,T}}\right)$. Setting ε to zero in Eqs. (5) and (6), one arrives at the median of F_y and E for different temperatures respectively.

The advantage of this setup is that, if no randomness is included in the generation of F_y and E, the analysis is equivalent to a deterministic approach and user-defined equations can be used for material properties. This way the user is not limited to EC3 material properties that was included in the original OpenSees code, and can use other available equations in the literature.

The flowchart in Fig. 18 shows the steps to perform thermal analysis for a given fire curve including uncertainties in the material properties. After the model is built, the random variables and related parameters are defined. Analysis is then performed in a "for-loop", where for every time step the following steps are performed:

(1) Input temperature for different layers of the cross section is calculated.
(2) F_y and E are randomly generated for the given temperatures.
(3) Parameters are updated with the newly calculated values of F_y and E.

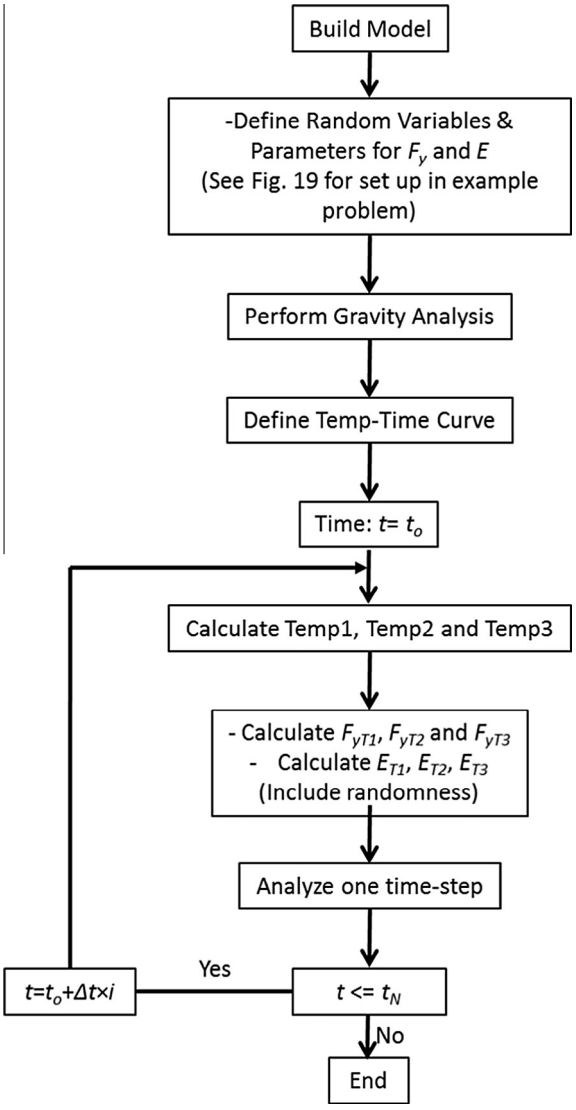

Fig. 18. Step-by-Step procedure to perform reliability analysis with the thermal module in OpenSees.

It should be noted that it is up to the user on how to include the randomness (ε in Eqs. (5) and (6)) in F_y and E which can be done by either (1) generating ε at every time step during the analysis of one full cycle of fire temperature–time curve (generating ε inside the for-loop), or (2) keeping ε the same for the duration of one full cycle of fire temperature–time analysis (generating ε before the for-loop starts). For steel structures, it is reasonable to keep the random variable ε constant in F_y, as well as E, for the duration of one fire curve analysis. Otherwise, as the temperature changes at each time step, the mechanical properties of steel can shift between values above and below the median.

5.3. Reliability example: 1MP perimeter column

The same example discussed in Section 3.1 is used as a sample study to perform reliability analysis in OpenSees. In the deterministic case, the 1MP column is modeled with 8 *dispbeamcolumnthermal* elements, and each element is made of 3 sections. Each section models the cross section with fibers, 4 fibers in each flange, and 8 fibers in the web, as shown in Fig. 19. The temperature gradient in the cross section is modeled using three temperature inputs (lumped masses), one for each flange, and one for the web according to Quiel and Garlock [27]. Consequently, the reduced values of F_y and E during the thermal analysis are different for the flanges and the web. Therefore, a total of 6 random variables should be defined for the analysis, three for F_y (two flanges and the web) and three for E (two flanges and the web). Finally, each random variable should be associated with a *Parameter*. For example, the first *Parameter* assigns F_y to the four fibers in the bottom flange over 3 sections and 8 elements along the column. A summary of the defined random variables and parameters are shown in Fig. 19.

The thermal analysis starts when all of the random variables and parameters are defined. Steel time–temperature curves are defined as an input to OpenSees. At the beginning of every time step, steel temperatures for the current time and different layers of the cross section are stored. As explained in Section 5.2, a tcl script is written to assign the time step and fire time–temperature curves as inputs for calculating the temperature for flanges and the web for the current time step. The temperatures are then used as inputs to another tcl script that calculate F_y and E based on Eqs. (5) and (6). In this example, it is assumed that the random variable ε in Eqs. (5) and (6) is constant during the analysis of one full fire temperature–time curve. As discussed in Section 5.2, both flanges and the web in the column is made of the same steel material, and is therefore expected to perform consistently in relation to the median values for all temperatures.

As part of the reliability analysis of 1MP column, 100 fire temperature–time curves are generated based on the 1MP fire [15]. The fire curves are generated by including uncertainties in fire load density. The detailed procedure for developing probabilistic temperature–time curves is explained in [9]. The maximum fire temperature T_{max} reached in each of 100 iterations is recorded. T_{max} has a minimum, maximum and the mean of 573, 1001, and 764 respectively. Fig. 20 shows the fire curves corresponding to the minimum, maximum, and the mean T_{max}. All considered fire curves fall in between the minimum and the maximum curves. Heat transfer analysis is performed using the MATLAB code discussed previously in Section 3.1. The steel time–temperature curves are defined as inputs to OpenSees.

The time of failure for the column, if the column fails, is recorded. The probability of failure is calculated to be 0.13 for the column. Fig. 21 shows the Cumulative Distribution Function (CDF) for failure time of the 1MP column. The results show that the column fails with a mean failure time of 43 min, and always in less than one hour. Since only 13 fire curves (out of 100) caused failure, the CDF curve is not smooth.

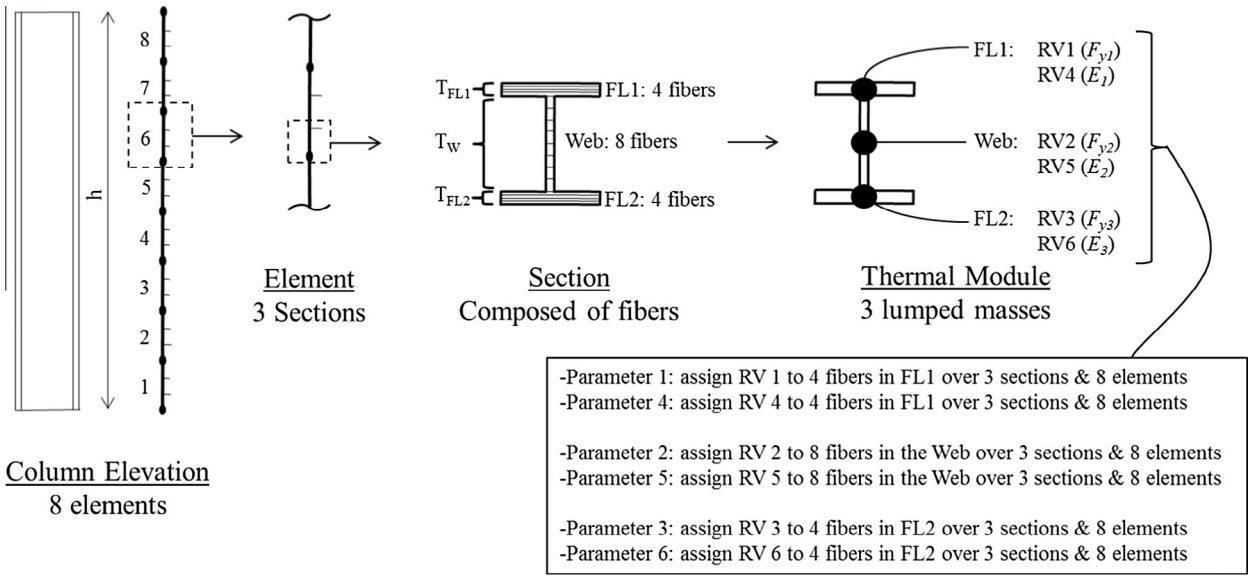

Fig. 19. Reliability setup for the 1MP perimeter column.

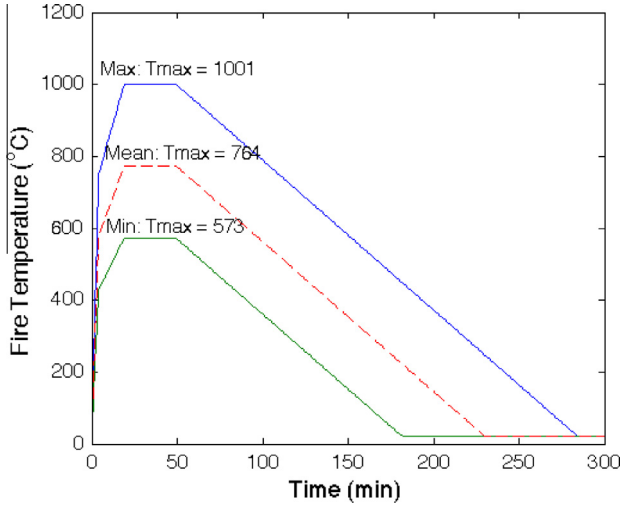

Fig. 20. Range of considered fire time–temperature curves.

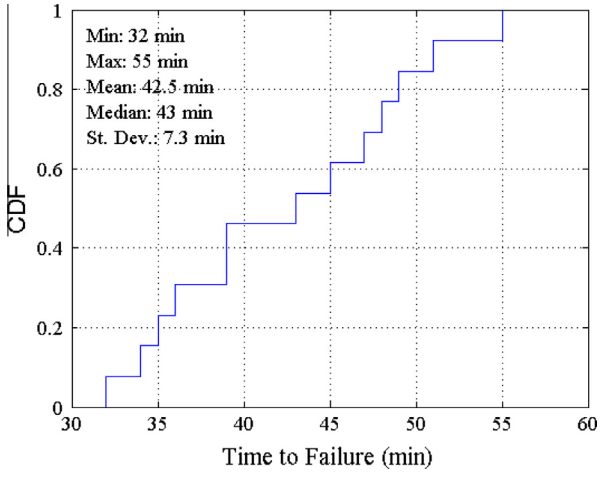

Fig. 21. Cumulative Distribution Function (CDF) for failure time of the 1MP perimeter column.

A similar probabilistic study was previously performed on the 1MP perimeter column using a MATLAB script [10]. The MATLAB script incorporated the uncertainties in fire load, mechanical and thermal properties of steel. In the MATLAB analysis, the probability of failure and the minimum time of failure were calculated with 1% and 5% margin of error respectively. The probability of failure was calculated as 0.29, and the minimum, maximum, mean and standard deviation of the failure time were calculated to be 24, 71, 47, and 9 respectively.

The results for failure time from the MATLAB script show close agreement with the implementation of reliability analysis in OpenSees. The probability of failure from the two studies is different (0.13 in OpenSees vs. 0.29 in MATLAB). The OpenSees example was run for 100 cases, whereas the MATLAB study implemented two termination criteria, as explained above, that were achieved after 2325 runs. Therefore, it is expected that fewer failure cases will be captured in 100 runs as compared to 2325 runs. This confirms the importance of setting convergence criteria in performing reliability analyses. Overall, the results illustrate that the enhanced version of OpenSees is working as intended.

6. Conclusions

The paper discussed the new modifications to the thermal module of OpenSees to enhance its fire analysis capabilities and make fire following earthquake (FFE) studies possible. The updates included (1) a strain-based formulation for the constitutive material model that considers strain reversals, and (2) calculation of moment about geometric centroid. Two validation studies were used to demonstrate the improvements in the fire module. A 9-story frame was also modeled and analyzed under fire following earthquake to demonstrate the multi-hazard capabilities of the modified OpenSees. Results show close agreement with other analysis tools and lend credibility to the use of modified OpenSees for seamless seismic-fire analysis.

The OpenSees source code with accompanying tcl scripts were used to perform reliability analysis of a structural member in OpenSees. The setup required the use of the currently available reliability module in OpenSees. Uncertainties in fire load density, steel yield strength, and modulus of elasticity were included in the analysis using stochastic models developed in previous studies

[9,10]. Reliability analysis was performed using Monte Carlo Simulations, where several temperature–time curves were developed as input based on uncertainties in fire load density. Uncertainties in mechanical properties of steel were considered through additional tcl scripts, in which these properties were calculated at every time step considering the uncertainty. The proposed procedure could also be used to perform deterministic analysis with user defined properties of steel at elevated temperatures, as is the current state-of-practice.

This work takes the currently available software OpenSees and modifies it to provide a tool for probabilistic fire and FFE analysis. The advantage of OpenSees, compared to other commercially available finite element programs, is that seismic and thermal analysis can be performed with reasonable computational resources. In addition, given that OpenSees is an open source program, the user has greater freedom to modify the source code for the purpose of the specific problem.

Acknowledgements

The authors would like to thank Professor Michael Scott of Oregon State University for his help and advice on the reliability module of OpenSees. Also, we would like to thank Professor Andre Barbosa of Oregon State University for his consultation on the OpenSees enhancements. Finally, we would like to thank Professor Asif Usmani and his research group at the University of Edinburgh, especially his student Liming Jiang, for their invaluable work in developing the thermal module in OpenSees, as well as their support of this study.

References

[1] AISC Steel Construction Manual. American Institute for Steel Construction. 13th ed.; 2010.
[2] AISC Seismic Provisions for Structural Steel Buildings (ANSI/AISC 341–10). Chicago (IL): American Institute of Steel Construction Inc.,; 2010.
[3] ASCE/SEI/SFPE 29-05. Standard calculation methods for structural fire protection. Reston (VA): Structural Engineering Institute, American Society of Civil Engineers; 2005.
[4] ASCE Minimum Design Loads for Buildings and Other Structures (ASCE/SEI 7-10). Reston (VA): American Society of Civil Engineers, 2010.
[5] ASTM E119. standardized test method for fire tests of building construction and materials. West Conshohocken (PA): American Society for Testing Materials; 2012.
[6] CEN. Eurocode3: design of steel structures, part 1–2: general rules – structural fire design (ENV 1993-1-2:2001). Brussels: European Committee for Standardization (CEN); 2001.
[7] CEN. Eurocode1: actions on structures, part 1–2: general actions – actions on structures exposed to fire. Brussels: Belgium: European Committee for Standardization (CEN); 2002.
[8] Della Corte G, Landolfo R, Mazzolani FM. Post-earthquake fire resistance of moment resisting steel frames. Fire Safety J 2003;38:593–612.
[9] Elhami Khorasani N, Garlock MEM, Gardoni P. Fire load: survey data, recent standards, and probabilistic models for office buildings. J Eng Struct 2014;58:152–65.
[10] Elhami Khorasani N, Gardoni P, Garlock MEM. Probabilistic fire analysis: material models and evaluation of steel structural members. J Struct Eng (ASCE) 2015. http://dx.doi.org/10.1061/(ASCE)ST.1943-541X.0001285.
[11] El-Rimawi JA, Burgess IW, Plank RJ. The treatment of strain reversal in structural members during the cooling phase of fire. J Constr Steel Res 1996;37(2):115–35.
[12] FEMA-350. Recommended seismic design criteria for new steel moment-frame buildings. Washington (DC): Prepared by the SAC Joint Venture for the Federal Emergency Management Agency; 2000.
[13] Franssen J-M. The unloading of building materials submitted to fire. Fire Saf J 1990;16:213–27.
[14] Franssen J-M. SAFIR: a thermal/structural program for modeling structures under fire. Eng J AISC 2005;42:143–58.
[15] Garlock MEM, Quiel SE. The behavior of steel perimeter columns in a high-rise building under fire. Eng J AISC 2007;44:359–72.
[16] Garlock MEM, Quiel SE. Mechanics of wide-flanged steel sections with thermal gradients due to fire exposure. Int J Steel Struct Korean Soc Steel Construct 2007;7(3):153–62.
[17] Garlock MEM, Quiel SE. Plastic axial load – moment interaction curves for fire-exposed steel sections with thermal gradients. J Struct Eng ASCE 2008;134(6):874–80.
[18] Ghojel JI, Wong MB. Three-sided heating of I-beams in composite construction exposed to fire. J Constr Steel Res 2005;61:834–44.
[19] Gupta A, Krawinkler H. Seismic demands for performance evaluation of steel moment resisting frame structures. Technical report 132. Stanford (CA): The John A. Blume Earthquake Eng Rsch Center, Dept of Civil Eng, Stanford University; 1999.
[20] Ibarra LF, Krawinkler H. Global collapse of frame structures under seismic excitations. Technical report 152. The John A. Blume Earthquake Engineering Rsch Center, Dept of Civil Eng, Stanford University; 2005.
[21] IBC: International Building Code. International code council. Suite 600, 5203 Leesburg Pike, Falls Church (VA) 22041; 2012.
[22] Jiang J, Jiang L, Kotsovinos P, Zhang J, Usmani A, McKenna F, et al. OpenSees software architecture for the analysis of structures in fire. J Comput Civ Eng ASCE 2015;29(1).
[23] Jiang J, Usmani A. Modeling of steel frame structures in Fire using OpenSees. J Comput Struct 2013;118:90–9.
[24] Lignos DG, Krawinkler H. Deterioration modeling of steel components in support of collapse prediction of steel moment frames under earthquake loading. ASCE J Struct Eng 2011;137(11):1291–302.
[25] McKenna F, Fenves GL. Opensees 2.4.0, Computer Software. UC Berkeley, Berkeley (CA); 2006. <http://opensees.berkeley.edu>.
[26] Quiel SE, Garlock MEM. A closed-form analysis of perimeter member behavior in a steel building frame subject to fire. Eng Struct 2008;30:3276–84.
[27] Quiel SE, Garlock MEM. Closed-form prediction of the thermal and structural response of a perimeter column in a fire. Open Construct Build Technol J 2010;4:64–78.
[28] Quiel SE, Garlock MEM. Parameters for modeling a high-rise steel building frame subject to fire. J Struct Fire Eng 2010;1(2):115–34.
[29] Rahnama M, Krawinkler H. Effect of soft soils and hysteresis models on seismic design spectra. Rep. No. TB 108. Stanford (CA): The John A. Blume Earthquake Engineering Center, Stanford University; 1993.
[30] Ronagh HR, Behnam B. Investigating the effect of prior damage on the post-earthquake fire resistance of reinforced concrete portal frames. Int J Concr Struct Mater 2012;6:209–20.
[31] Rubert A, Schaumann P. Tragverhalten stahlerner Rahmensysteme bei Brandbeanspruchung. Stahlbau 1985;9.
[32] Rubert A, Schaumann P. Structural steel and plane frame assemblies under fire action. Fire Saf J 1986;10:173–84.
[33] SAC Joint Venture. FEMA 355C: state of the art report on system performance of steel moment frames subject to earthquake ground shaking. Federal Emergency Management Agency; September, 2000.
[34] Scawthorn C, Eidinger JM, Schiff AJ. Fire following earthquake. Technical council on lifeline earthquake engineering, Monograph No. 26. Reston: Published by the American Society of Civil Engineers; 2005.
[35] Scott MH, Haukaas T. Software framework for parameter updating and finite-element response sensitivity analysis. J Comput Civ Eng 2008;22:281–91.
[36] Scott MH, Mackie KR. Summary of work on OpenSees reliability/optimization/sensitivity. PEER Research, part of OpenSees source code packag; November 2012.
[37] Somerville P, Smith N, Punyamurthula S, Sun J. Woodward-clyde federal services. Development of ground motion time histories for phase 2 of the FEMA/SAC Steel Project, BD-97/04 SAC joint venture; 1997.
[38] UoE OpenSees wiki. Edinburgh University – OpenSees Developers, 2014. <https://www.wiki.ed.ac.uk/display/opensees/UoE+OpenSees>.
[39] Zaharia R, Pintea D. Fire after earthquake analysis of steel moment resisting frames. Int J Steel Struct KSSC 2009;9:275–84.